

**Gulf Stream drives Kuroshio behind the recent abnormal ocean warming**

**Yoko Yamagami<sup>1</sup>, Hiroaki Tatebe<sup>1</sup>, Tsubasa Kohyama<sup>2</sup>, Shoichiro Kido<sup>1</sup>, Satoru Okajima<sup>3</sup>**

<sup>1</sup>Japan Agency for Marine-Earth Science and Technology, Yokohama, Japan

<sup>2</sup>Department of Information Sciences, Ochanomizu University, Tokyo, Japan

<sup>3</sup>Institute of Life and Environmental Sciences, University of Tsukuba, Tsukuba,  
Japan

Corresponding author: Yoko Yamagami ([y.yamagami@jamstec.go.jp](mailto:y.yamagami@jamstec.go.jp))

†Research Center for Environmental Modeling and Application, Japan Agency for Marine-Earth Science and Technology, 3173-25 Showamachi, Kanazawaku, Yokohama, Kanagawa 236-0001, Japan

## **Abstract**

The abnormal ocean warming has manifested in coherent sea surface temperature (SST) anomalies over the Northern Hemisphere mid-latitudes in recent years. However, the causality remains poorly understood behind inter-basin interactions between the North Pacific and North Atlantic. Here we show that SST variability in the Gulf Stream region drives the internal SST variability in the Kuroshio region in climate model simulations, but the opposite does not hold. Anomalous SSTs in the Gulf Stream induce wind anomalies in the North Pacific, associated with the Northern Annular Mode (NAM), and facilitate oceanic Rossby wave adjustments in the Kuroshio Extension. Additionally, state-of-the-art climate models with high spatial resolution oceans capture the “North Atlantic SST-NAM coupling” better than models with coarse resolution oceans. These findings highlight the critical role of internal North Atlantic variability as a pacemaker of mid-latitude climate, contributing to the recent abnormal ocean warming in the Northern Hemisphere.

## **Main**

The global mean temperature has reached the record high in 2023 and 2024<sup>1-6</sup>. The impact of global warming has emerged as severe marine heatwaves in the global oceans<sup>7</sup>, and the abnormal sea surface temperature (SST; Supplementary Fig. 1) anomalies contribute to extreme summer heatwaves over the mid-latitude ocean<sup>8-10</sup>. In addition to global warming<sup>11</sup>, mid-latitude's climate system varies internally<sup>12-15</sup>, necessitating an understanding of the dynamical mechanisms underlying the internal climate variability. Although natural climate variability in the tropical Pacific oceans is known as a pacemaker of global climate<sup>16,17</sup>, the impact of mid-latitude ocean on large-scale climate has also been recognized in recent decades<sup>18,19</sup>. However, climate models in Coupled Model Intercomparison Project Phase 6 (CMIP6) underestimates the potential predictability of mid-latitude climate<sup>20,21</sup>, and thus, understanding and predicting the mid-latitude climate system remains challenging<sup>22</sup>.

The Kuroshio and Gulf Stream, major western boundary currents crucial to the Northern Hemispheric climate system, are characterized by their sharp currents and mesoscale eddies. SST anomalies and their gradient in western boundary regions influences not only surface boundary layer<sup>23</sup> but also deep convection<sup>24</sup>, storm track

activity<sup>25-27</sup>, North Atlantic Oscillation (NAO)<sup>28,29</sup>, and the Northern Hemisphere annular mode (NAM)<sup>30,31</sup>. However, since mid-latitude SSTs have been considered passive to stochastic atmospheric variability, how Kuroshio and Gulf Stream affect each other has been largely unexplored, except for the followings. Possibility of dynamical connections between the western boundary currents was suggested based on a simple linear model with air-sea interaction<sup>32</sup> and analysis of observational data<sup>33</sup>. A climate model simulation demonstrated a delayed response about five-year in the Kuroshio Extension following the Atlantic Multidecadal Variability (AMV)<sup>34</sup>. More recent studies using high-resolution climate models, combined with observations and a simple theoretical model, have indicated the potential synchronous co-variability between the Kuroshio and the Gulf Stream<sup>35</sup>.

Variability in the western boundary current regions is dominated by oceanic Rossby waves and the thermal memory will continue about several years<sup>15,36</sup>, potentially serving as a source of natural variability in the mid-latitude climate. Therefore, the interaction between Kuroshio and the Gulf Stream<sup>32-35</sup> could be a predominant source of decadal predictability in the Northern Hemisphere climate system. However, the causal relationships between these currents and their dynamical mechanism remain unclear. To this end, we investigate climate simulations in which SST anomalies in Kuroshio and Gulf Stream regions are constrained with various climate model configurations. These experiments suggest dynamical relationship that Gulf Stream actively leads to decadal Kuroshio variations via NAM-like atmospheric circulation anomalies and the influence of North Atlantic SST contributes to the recent abnormal ocean warming.

### **North Atlantic/Pacific-Global Atmosphere experiment**

To examine the mutual impact of Kuroshio and Gulf Stream SSTs, a series of ensemble experiments were conducted using Model for Interdisciplinary Research on Climate version 6 (MIROC6<sup>37</sup>), a climate model participating in CMIP6<sup>38</sup>. The reference experiment (CTL) is a pre-industrial simulation spanning 100 years with a globally eddy-permitting ocean resolution. Additional ensemble experiments, similar to CTL, constrain SSTs in the North Pacific or North Atlantic with SST anomalies derived from CTL. These experiments consist of 5 ensemble members and are referred to as

North Pacific-Global Atmosphere (NPGA) and North Atlantic-Global Atmosphere (NAGA), respectively (Methods). When SST variations in the Kuroshio or Gulf Stream regions are constrained, the correlations between the area-averaged SSTs from the ensemble mean and CTL exceed 0.94 (Supplementary Fig. 3).

The comparative analysis reveals that low-frequency variations in Kuroshio SSTs (140°E-170°E, 35°N-45°N) are attributed to Gulf Stream SSTs (50°-80°W, 35°N-45°N) (Figure 1). A significant correlation is observed between Kuroshio SST in CTL and that of the ensemble mean for NAGA ( $r = 0.38$ ), whereas Gulf Stream SST variations in NPGA are virtually uncorrelated with those in CTL ( $r = 0.098$ ). The correlation increases notably when comparing the 5-year low-pass filtered time series ( $r = 0.51$ ; Supplementary Fig. 4), suggesting low-frequency coherent variability<sup>35</sup>. In CTL, the Kuroshio and Gulf Stream SSTs exhibit significant positive correlations when the Gulf Stream leads by 1 to 4 years (Figure 1c). This lead-lag relationship is also evident in NAGA, while NPGA fails to capture it, supporting forcing of the Gulf Stream on Kuroshio. It is worth mentioning that significant negative SST anomalies appear in the subpolar gyre for NAGA, where SST anomalies are not directly constrained (Figure 1g,h).

Interestingly, the causal relationship between the Gulf Stream and Kuroshio is not clearly represented in the non-eddy ocean model experiment, even though the North Atlantic SST variability is constrained by the CTL in NAGA-LR (Figure 1d). The correlation of Kuroshio SST in NAGA-LR and CTL is not significant ( $r = 0.15$ ), and the increase in lag correlations with 1- to 4-year Gulf Stream lead is not represented. Also, SST anomalies are not significant in the subpolar gyre, indicating that NAGA-LR fails to constrain the subpolar SST variability. The NPGA-LR shows weak remote influence of the Kuroshio (Figure 1e), which is consistent with NPGA.

The Singular Value Decomposition (SVD) analysis is applied to the ensemble mean of North Pacific (120°E-180°E, 25°N-55°N) and North Atlantic (30°W-90°W, 25°N-55°N) SST anomalies (Methods), and shows that only NAGA captures in-phase Kuroshio and Gulf Stream SST co-variations on decadal timescales. In CTL, in-phase SST co-variations between the Kuroshio and Gulf Stream are extracted as the first SVD mode (Supplementary Fig. 5a,  $r = 0.48$ ), which is associated with their meridional shifts. Similar SST co-variations are also extracted as the first mode exclusively in

NAGA (Supplementary Fig. 5;  $r=0.43$ ). These anomalies are prominent north of the Kuroshio Extension and in the eastern part of the Gulf Stream Extension, although positive anomalies near the U.S. east coast are relatively small. In contrast, NPGA and NPGA-LR both capture an anti-phase SST pattern as the first SVD mode. Although the first SVD mode in NAGA-LR shows in-phase co-variation, the correlation between the associated time series is smaller than NAGA (Supplementary Fig. 5;  $r = 0.29$ ), indicating a predominant Gulf Stream influence on the Kuroshio due to the eddy-permitting oceanic resolution.

Wavelet analysis of SST anomalies further supports the causality, demonstrating that constraining Gulf Stream SST reproduces decadal variations in Kuroshio SST, but not vice versa (Supplementary Fig. 6). In CTL, both Kuroshio and Gulf Stream SSTs exhibit significant decadal-scale variability. The significant decadal variability is reproduced in the ensemble mean of Kuroshio SST in NAGA but not in the Gulf Stream SST in NPGA (Supplementary Fig. 6c, d). While NAGA-LR exhibits significant interdecadal variability, the structure of power peaks is inconsistent compared to CTL and NAGA. The results highlight a causal relationship where Gulf Stream SST drives Kuroshio SST variability at decadal-to-interdecadal timescales. Therefore, the next section will focus on the physical mechanisms through which Gulf Stream SST influences Kuroshio SST variations, primarily in NAGA.

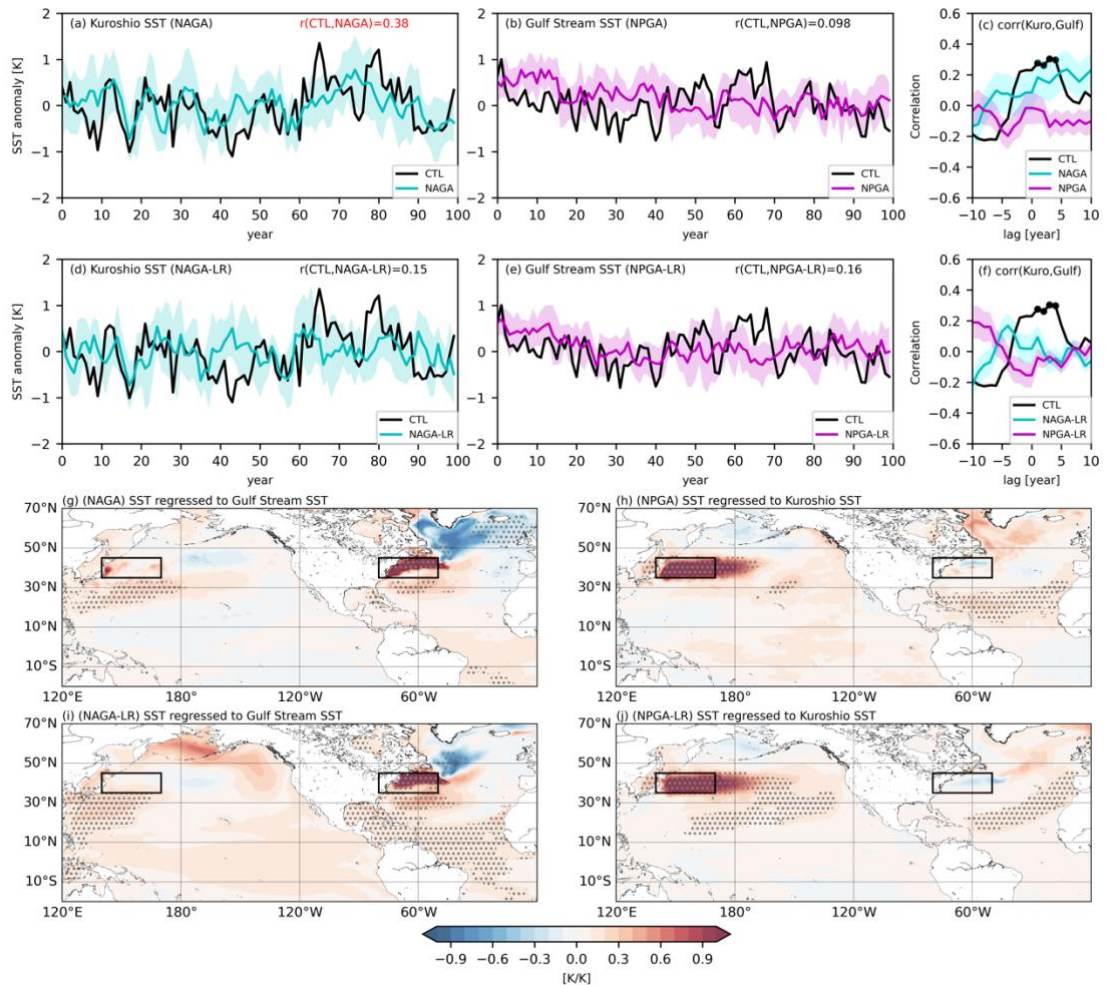


**Figure 1. Simulated impacts of SSTs in the Kuroshio and Gulf Stream on each other.** a Annual mean SST anomalies averaged over the Kuroshio region ( $140^{\circ}\text{E}$ - $170^{\circ}\text{E}$ ,  $35^{\circ}\text{N}$ - $45^{\circ}\text{N}$ ; the region is indicated with a box in g-j) based on CTL (black) and the ensemble means for NPGA (magenta) and NAGA (cyan). Shading indicates one standard deviation of ensemble members in both experiments. Correlation coefficient for CTL and NAGA is shown in the upper right, with red colors indicating the statistically significant at 90% confidence level. b As in a, but for SST anomalies averaged over the Gulf Stream region ( $30^{\circ}$ - $80^{\circ}\text{W}$ ,  $30^{\circ}$ - $50^{\circ}\text{N}$ ; black box in g-j). c Lag-correlation of the annual mean Kuroshio and Gulf Stream SST anomalies for CTL (black) and ensemble means of NPGA (magenta) and NAGA (cyan). Black dots are statistically significant correlations for CTL. Shading indicates one standard deviation of ensemble members. d-f As in a-c, but for NPGA-LR and NAGA-LR. g,h Linear regression of annual mean SST anomalies to the time series of SST anomalies in (g) the Gulf Stream SST for NAGA and (h) the Kuroshio

SST for NPGA. i,j As in g,h, but for (i) NAGA-LR and (k) NPGA-LR.

### **Mechanisms for decadal variations in Kuroshio Extension**

We analyze the mechanism of Kuroshio SST variations primarily in NAGA, and demonstrate that wind stress anomalies in the North Pacific lead to SST variations via oceanic Rossby wave adjustment in the Kuroshio Extension. This mechanism is evident in low-frequency westward SST and SSH propagations in the Kuroshio Extension clearly observed in CTL and NAGA (Fig. 2a,b; Supplementary Fig. 7). In both CTL and NAGA, SSH anomalies originating in the central North Pacific propagate westward, consistent with observations and linear baroclinic Rossby wave theory<sup>39,40</sup>. The lack of a clear westward-propagating signal in NAGA-LR can be attributed to two factors. First, wind stress anomalies are not represented in the North Pacific, preventing the generation of linear Rossby waves. Second, NAGA-LR fails to represent jet-trapped Rossby waves<sup>41-43</sup> due to its coarse resolution. It is worth noting that individual Rossby wave propagation in CTL and NAGA does not fully correspond, owing to differences in atmospheric stochastic forcing, which can either trigger or hinder oceanic Rossby wave. Nevertheless, the ensemble mean for NAGA captures SST and SSH variability in the Kuroshio Extension for CTL (Supplementary Fig. 8). In the Kuroshio Extension, SSH and SST anomalies in NAGA significantly correlate with those in CTL, whereas NAGA-LR fails.

An examination of the ocean mixed-layer heat budget (Methods) reveals that ocean dynamics enhance Kuroshio SST variations associated with Gulf Stream SST, whereas surface heat fluxes dampen the SST tendency (Fig. 2). Kuroshio SST variations can be explained by the cumulative temperature tendency in the ocean mixed layer. Ocean dynamics contributions, including horizontal advection and entrainment, show a positive correlation with mixed-layer temperature tendency ( $r = 0.63$ ), while the heat flux term shows a negative correlation ( $r = -0.48$ ).

Each contribution of the mixed-layer heat budget regressed to Gulf Stream SST anomalies reveals that wind stress curl anomalies over the North Pacific sustain ocean dynamics-induced temperature anomalies for about five years (Fig. 2d). When Gulf Stream SST anomalies are positive, anticyclonic wind stress anomalies are evident in

the North Pacific, i.e., a weakening of the Aleutian Low. Wind stress curl anomalies over the western to central North Pacific trigger westward Rossby waves. Over 1-5 years, positive SSH anomalies persist offshore east of Japan, consistent with lead-lag relationship with the significant lag-correlation between Kuroshio and Gulf Stream SST (Fig. 1c). These SSH anomalies induce anticyclonic surface ocean circulation anomalies, enhancing the advection of Kuroshio-origin warm water masses northward along the Japanese coast ( $35^{\circ}\text{N}$ - $45^{\circ}\text{N}$ ). Consequently, horizontal advection contributes to the positive mixed-layer temperature tendency in the Kuroshio/Oyashio mixed water region. Furthermore, these temperature anomalies expand eastward along the Oyashio Current, leading to the development of large-scale SST anomalies over the western North Pacific.

Recent studies suggest that the northward shift in the latitude of Kuroshio separation is caused by Rossby wave propagation induced by wind stress anomalies, aligning with the mechanism proposed in this study. However, it should be noted that the ocean model used here has a  $0.25^{\circ}$  horizontal resolution, and it remains unclear whether the model fully captures the dynamics of Kuroshio separation. Therefore, further investigations using higher-resolution models are necessary to clarify the detailed mechanisms.





values. c Time series of SST (gray) and time-integrated temperature tendency (black) vertically integrated within the mixed layer (top) [K], while the temperature tendency (black) [ $10^{-7}\text{Ks}^{-1}$ ], surface heat flux contribution (magenta), and oceanic contribution (cyan) vertically integrated within the mixed layer (bottom) for NAGA. d Lag-regressions of annual mean temperature tendency, heat flux contribution, and ocean contribution to the mixed layer temperature tendency averaged within the mixed layer [ $10^{-7}\text{Ks}^{-1}/\text{K}$ ]. SSH (shade) [cm/K], surface velocity (contours) [ $\text{cm s}^{-1}/\text{K}$ ], and wind stress (vectors) [ $\text{dyn cm}^{-2}/\text{K}$ ] are also shown (right figures). The dots and vectors indicate statistically significant regression coefficients. The black dashed box shows the Kuroshio region. The positive (negative) lag means that Gulf Stream SST leads (delays).

### **Active influence of North Atlantic SST on Northern Hemisphere circulation anomalies**

Comparison of NAGA and NPGA suggests that Kuroshio SST anomalies are attributed to wind stress anomalies over the North Pacific caused by Gulf Stream SST variability over the North Atlantic. This result suggests the existence of hemispheric-scale atmospheric circulation anomalies associated with North Atlantic SST variability. Basin-scale North Atlantic SST variability, such as the AMV, is thought to influence the North Pacific via the Walker circulation and equatorial Rossby waves<sup>44-48</sup>, or mid-latitude atmospheric teleconnection<sup>30,31,34</sup>. Thus, here we analyze the relationship between Gulf Stream SSTs and North Pacific atmospheric circulation anomalies, focusing on two possible pathways: tropical and extratropical routes.

To evaluate the forcing of Gulf Stream SST variability on the large-scale atmospheric circulation, we regressed atmospheric circulation anomalies onto Gulf Stream SST during boreal winter (DJF: December-January-February) for NAGA and NAGA-LR (Fig. 3). In both CTL (Supplementary Fig. 9) and NAGA, a meridional dipole pattern over the North Atlantic and a weakening of the Aleutian Low over the North Pacific are evident. A northward shift of storm tracks is observed both in the North Atlantic and the Pacific, suggesting the mid-latitude atmospheric teleconnections<sup>34</sup>. Positive (negative) geopotential height anomalies in the mid-latitudes (Arctic) in the ensemble mean of NAGA indicate that Gulf Stream SST anomalies trigger hemispheric-scale response that projects onto the Northern Annular Mode (NAM).

In NAGA-LR, the NAM-like response is less distinct. The meridional dipole structure over the North Atlantic is weaker, and the Aleutian Low rather strengthens unlike in NAGA, suggesting that wind stress anomalies fail to significantly influence the Kuroshio Extension. These differences between NAGA and NAGA-LR likely stem from coupled atmosphere-ocean processes in the North Atlantic to be discussed later.

The robustness of the active influence of Gulf Stream SST on the NAM-like response is examined through additional sensitivity experiments. First, we conduct experiments where SST anomalies in the tropical Indo-Pacific regions are restored to climatology (Methods; CTL-NoINPAC and NAGA-NoINPAC in Supplementary Fig. 2) to suppress the impact of tropical SST forcing. The results show a weakening of the Aleutian Low associated with Gulf Stream SST anomalies similar to CTL and NAGA (Supplementary Fig. 10). The NAM-like spatial pattern persists from the surface to the troposphere without tropical SST forcing, indicating that the NAM-like response is primarily due to the extratropical SST forcing. However, reduced amplitude and differences in the spatial pattern, particularly in the stratosphere, suggest that tropical SSTs still play a non-negligible role. For example, in NAGA, tropical Pacific SST anomalies are slightly negative when Gulf Stream SST anomalies are positive (Figure 1g). Thus, the weaker response in NAGA-NoINPAC implies that the tropical SST forcing is a supporting factor in forming anticyclonic anomalies over the central North Pacific.

Notably, these NAM-like patterns exhibit significant anomalies not only in the troposphere but also in the stratosphere (Fig. 3a,b). The stratospheric NAM-like structure is shown to be linked to polar vortex anomalies and their downward influence on the mid-latitude troposphere<sup>30,49–51</sup>, inducing anticyclonic anomalies and meridional shifts in the westerlies over the Pacific sector.

We also conduct atmospheric model sensitivity experiments to test whether NAM-like atmospheric circulation anomalies are forced by SST anomalies, particularly in the North Atlantic (Fig. 3c,d). In these AGCM experiments, positive SST anomalies obtained as a regression SST pattern of global ocean onto the Gulf Stream SST are prescribed and compared to a control experiment forced by climatological SST and sea ice (Supplementary Fig. 11; Methods). Global SST anomalies reproduce the hemispheric atmospheric circulation anomalies seen in NAGA, suggesting that the NAM-like anomalies are actively driven by SST anomalies in NAGA (Fig. 3c). Positive

North Atlantic SST anomalies strengthen the polar vortex, leading to distinct NAM-like anomalies extending from the stratosphere to the upper troposphere (AGCM-Gulf\_SST; Fig. 3d). Conversely, in the North Pacific, westerly anomalies in the lower troposphere and Aleutian Low near the surface are weaker than those of NAGA, likely due to the reduced thermal damping mechanism<sup>52-54</sup> by the fixed SST without the air-sea interaction. This evidence indicates the significant role of local air-sea interaction for NAGA, particularly in the Kuroshio Extension region. In fact, consistent with previous studies<sup>55,56</sup>, NPGA and NPGA-LR in which SST anomalies in the Kuroshio region are constrained demonstrated that positive Kuroshio SST anomalies lead to weakening of the Aleutian Low (Supplementary Fig. 12). We note that the stratospheric response in CTL differs from those in NAGA and AGCMs, likely due to internal variability in CTL. By calculating the ensemble mean with SST-restoring or fixed SST in the North Atlantic, the stratospheric pathway has emerged in the NAGA and AGCM experiments.

In summary, Gulf Stream SST anomalies influence wind stress curl anomalies in the North Pacific via a NAM-like response. The set of sensitivity experiments highlights the importance of extratropical air-sea coupling processes, particularly: the annular mode formation in both the troposphere and stratosphere triggered by North Atlantic SST anomalies, and local air-sea interactions in the Kuroshio Extension region. Previous studies suggest that AMV-related SST anomalies induce polar vortex changes through upward planetary wave propagation, leading to downward influence of annular mode toward the troposphere<sup>49-51,57,30,31</sup>. While the SST anomaly pattern focused by this study is close to the tripole rather than AMV, similar dynamical mechanisms underlying the NAM formation may help to understand the Gulf Stream-Kuroshio SST connection. Furthermore, these results are attributed to the characteristics of our experiments, including high-resolution ocean model, high-top atmospheric model, and the constraint of SST anomalies limited to the vicinity of the Gulf Stream. Consequently, it is likely that models in previous studies may not have fully captured the pathway through the stratosphere.

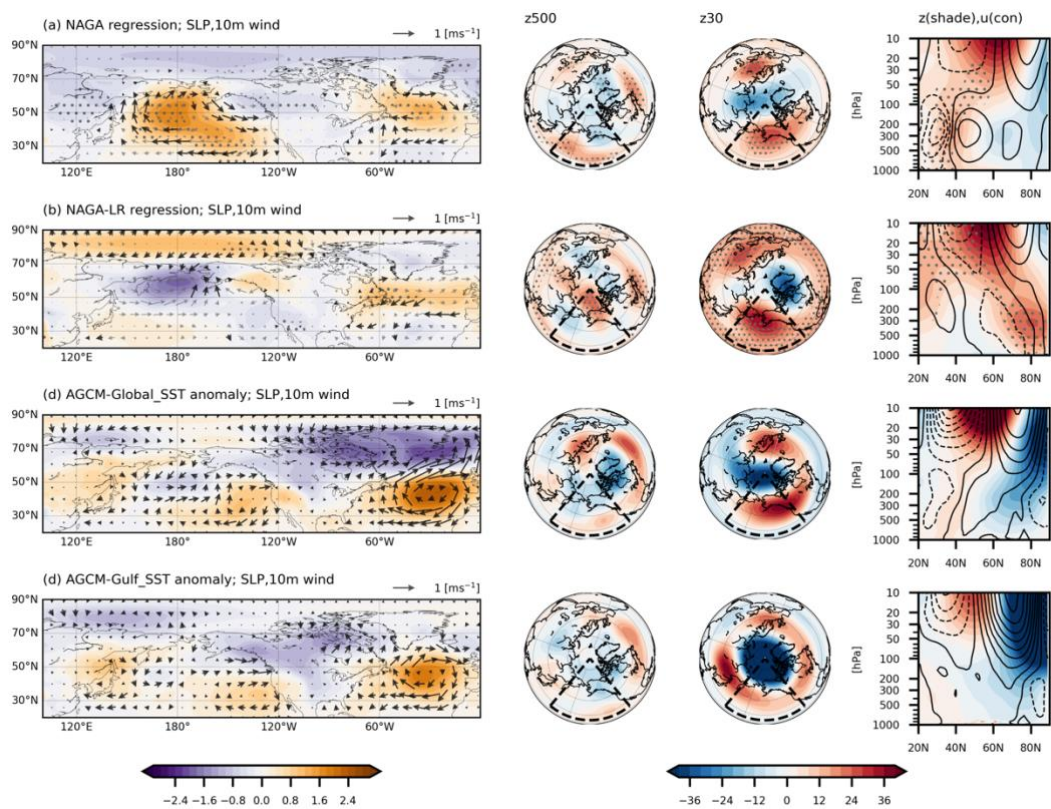


**Figure 3. Response of the surface, tropospheric, and stratospheric circulation anomalies associated with the Gulf Stream SST anomalies.** **a** Regression coefficients of DJF mean SLP (shade) [hPa/K] and 10m wind (vector) [ $\text{m s}^{-1}/\text{K}$ ], geopotential height at 500hPa [m/K], geopotential height at 30hPa [m/K], and zonally averaged geopotential height (shade) [m/K] and zonal velocity (contour) [ $\text{m s}^{-1}/\text{K}$ ] (right) for NAGA. All variables are regressed to the DJF mean SST anomalies in the Gulf Stream. Dots and black vectors mean the statistically significant regression coefficients. Zonal-average are calculated over the North Pacific region ( $140^{\circ}\text{E}$ - $140^{\circ}\text{W}$ ,  $20^{\circ}\text{N}$ - $90^{\circ}\text{N}$ ; black dashed boxes in the second and third panels). **b** As in **a**, but for **(b)** NAGA-LR. **c,d** As in **a**, but for anomalies for **(c)** AGCM-Global\_SST and **(d)** AGCM-Gulf\_SST from AGCM-Clim.

### Relationship between North Atlantic SST and Northern Annular Mode simulated in high-resolution models

To test the robustness of the dependence of atmospheric responses to Gulf Stream SST on ocean model resolution, we perform a multi-model analysis of CMIP6 data. The relationships between Gulf Stream SST and North Atlantic atmospheric response are

analyzed using multiple climate models from HighResMIP<sup>58,59</sup> (Methods) as well as CTL and CTL-LR (Fig. 4). In high-resolution (ocean eddy-permitting) models, positive Gulf Stream SST anomalies are associated with the typical positive NAM-like pattern. This pattern is characterized by a dipole structure over the North Atlantic, negative anomalies in the Arctic, and positive anomalies over the North Pacific, consistent with reanalysis. Conversely, in low-resolution (ocean non-eddy-permitting) models, the link is less distinct.

A key difference between NAGA and NAGA-LR simulations is observed in the North Atlantic Subpolar Gyre SST anomalies (Fig. 1). The resolution dependence of the “Gulf Stream SST-NAM” relationship in CMIP6 models is likely attributed to the formation of the dipole-shaped SST anomalies in the North Atlantic (Supplementary Fig. 13) that are realistically represented in high-resolution models<sup>60</sup>. Correlation analysis between Gulf Stream SST, Subpolar Gyre SST, and the NAO index supports this hypothesis (Fig. 4c). Eddy-permitting models tend to capture the stronger negative Gulf Stream-Subpolar Gyre SST correlation as well as the relationship between Gulf Stream SST and the NAO.

It is important to note that coupled model simulations do not necessarily clarify the causal relationship between North Atlantic SST and the NAM-like atmospheric response. Under pre-industrial control or 1950-control conditions, the atmosphere and ocean interact mutually, with the ocean often passively responding to the atmospheric internal variability. Consequently, the link between Gulf Stream SST and atmospheric circulation particularly in the stratosphere is not robustly clear in CMIP6 models (Supplementary Fig. 14). However, the resolution dependence found in NAGA and NAGA-LR suggests that Gulf Stream SST variability acts as a significant pacemaker for North Atlantic air-sea coupled variability, and further highlights the active influence of extratropical SSTs, which is also evident in the CMIP6 multi-model ensemble.



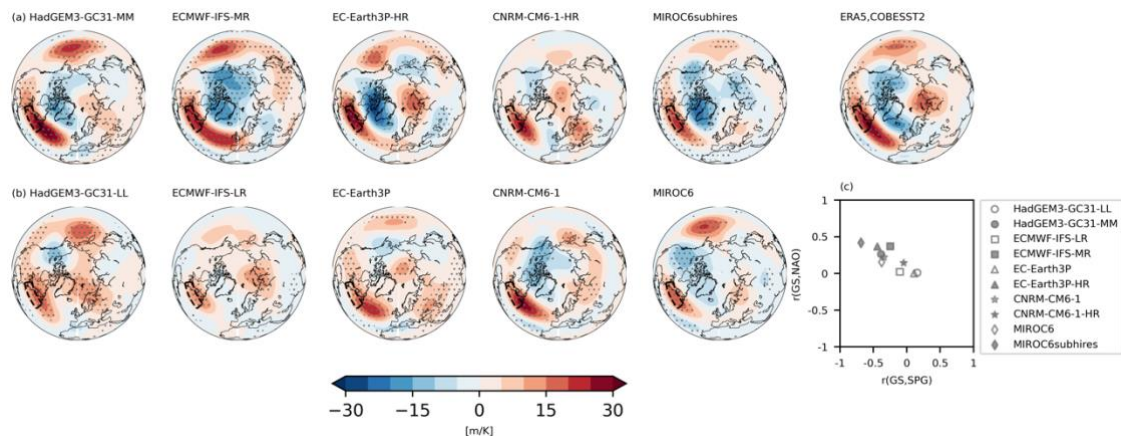


**Figure 4. Resolution dependence of the tropospheric circulation response to the Gulf Stream SST anomalies for CMIP6 models. a,b** DJF mean geopotential height at 500hPa [m/K] regressed to the DJF mean SST anomalies in the Gulf Stream (black dashed box) for CMIP6 models with (a) eddy-permitting and (b) non-eddy-permitting ocean model resolution (Methods). Dots indicate the statistically significant regression coefficients. c Scatter plots between the correlation coefficients DJF Gulf Stream SST for Subpolar Gyre SST (horizontal axis) and NAO index (vertical axis) for each CMIP6 model. Black (white) symbols indicate eddy-permitting (non-eddy-permitting) ocean resolution.

## Discussion

This study demonstrates a causal relationship in which Gulf Stream SST drives decadal variability in Kuroshio SST. It also reveals a dynamical mechanism whereby North Atlantic SST actively triggers NAM-like atmospheric responses, leading to wind stress anomalies over the North Pacific that modulate Rossby wave adjustments in the Kuroshio Extension. These findings revisit a previous study suggesting that the North Atlantic SST variability influences the Kuroshio Extension, and further propose that North Atlantic forcing exerts the effects via polar stratospheric variations, which are well-represented in climate models with high-resolution ocean components.

The proposed mechanisms help to understand the recent abnormal ocean warming observed in the Northern Hemisphere mid-latitude (Supplementary Fig.15). From 2019 to 2020, positive (negative) SST anomalies are observed in the subtropical (subpolar) North Atlantic. These SST anomalies are favorable to a positive NAO development from late 2019 to early 2020. Similar to the response in NAGA, negative anomalies are found

in the entire Arctic region, while anticyclonic anomalies in the mid-latitudes of the North Pacific. As a result, positive SSH anomalies develop and propagate westward since early 2020 in the central to western Kuroshio Extension region (around 160°E–150°W), sustaining positive SSH anomalies east of Japan from 2021 onwards. The positive SSH anomalies in recent years potentially contributes to northward shifts of the Kuroshio<sup>61</sup> and associated record-breaking heatwaves in East Asia<sup>62</sup>. While the global high temperatures observed in 2023 may primarily reflect a combination of global warming and the tropical climate variability<sup>8,9</sup>, we suggest that decadal variability originating in the North Atlantic could significantly contribute to anomalously high SSTs across the North Pacific midlatitude ocean.

Such extreme warming events pose significant risks to marine ecosystems and could have severe impacts on socioeconomic activities. It is therefore critical to investigate whether the mechanisms proposed in this study might intensify as a response to global warming and to investigate their ecological and societal implications. Moreover, this study implies that high-resolution climate models could enhance decadal prediction ability for the Northern Hemisphere and may provide solutions to challenges common in climate modeling, such as the signal-to-noise paradox.

## Reference

1. WMO confirms that 2023 smashes global temperature record. *World Meteorological Organization* <https://wmo.int/news/media-centre/wmo-confirms-2023-smashes-global-temperature-record> (2024).
2. WMO confirms 2024 as warmest year on record at about 1.55°C above pre-industrial level. *World Meteorological Organization* <https://wmo.int/news/media-centre/wmo-confirms-2024-warmest-year-record-about-155degc-above-pre-industrial-level> (2025).
3. Esper, J., Torbenson, M. & Büntgen, U. 2023 summer warmth unparalleled over the past 2,000 years. *Nature* **631**, 94–97 (2024).
4. Goessling, H. F., Rackow, T. & Jung, T. Recent global temperature surge intensified by record-low planetary albedo. *Science* **387**, 68–73 (2025).
5. Minobe, S. *et al.* Global and Regional Drivers for Exceptional Climate Extremes in 2023-2024: Beyond the New Normal. Preprint at <https://doi.org/10.21203/rs.3.rs->



- 5454786/v1 (2024).
6. Tsuchida, K., Kosaka, Y. & Minobe, S. The triple-dip La Niña was key to Earth's extreme heat uptake in 2022-2023. Preprint at <https://doi.org/10.21203/rs.3.rs-5597161/v1> (2025).
  7. Frölicher, T. L., Fischer, E. M. & Gruber, N. Marine heatwaves under global warming. *Nature* **560**, 360–364 (2018).
  8. Raghuraman, S. P. *et al.* The 2023 global warming spike was driven by the El Niño–Southern Oscillation. *Atmospheric Chem. Phys.* **24**, 11275–11283 (2024).
  9. Samset, B. H., Lund, M. T., Fuglestad, J. S. & Wilcox, L. J. 2023 temperatures reflect steady global warming and internal sea surface temperature variability. *Commun. Earth Environ.* **5**, 1–8 (2024).
  10. Voosen, P. El Niño fingered as likely culprit in record 2023 temperatures. *Science* **386**, 137–137 (2024).
  11. Wu, L. *et al.* Enhanced warming over the global subtropical western boundary currents. *Nat. Clim. Change* **2**, 161–166 (2012).
  12. Minobe, S. A 50–70 year climatic oscillation over the North Pacific and North America. *Geophys. Res. Lett.* **24**, 683–686 (1997).
  13. Latif, M. & Barnett, T. P. Causes of Decadal Climate Variability over the North Pacific and North America. *Science* **266**, 634–637 (1994).
  14. Latif, M. & Barnett, T. P. Decadal Climate Variability over the North Pacific and North America: Dynamics and Predictability. (1996).
  15. Griffies, S. M. & Bryan, K. Predictability of North Atlantic Multidecadal Climate Variability. *Science* **275**, 181–184 (1997).
  16. Kosaka, Y. & Xie, S.-P. Recent global-warming hiatus tied to equatorial Pacific surface cooling. *Nature* **501**, 403–407 (2013).
  17. England, M. H. *et al.* Recent intensification of wind-driven circulation in the Pacific and the ongoing warming hiatus. *Nat. Clim. Change* **4**, 222–227 (2014).
  18. Kwon, Y.-O. *et al.* Role of the Gulf Stream and Kuroshio–Oyashio Systems in Large-Scale Atmosphere–Ocean Interaction: A Review. *J. Clim.* **23**, 3249–3281 (2010).
  19. Kelly, K. A. *et al.* Western Boundary Currents and Frontal Air–Sea Interaction: Gulf Stream and Kuroshio Extension. (2010) doi:10.1175/2010JCLI3346.1.

20. Smith, D. M. *et al.* North Atlantic climate far more predictable than models imply. *Nature* **583**, 796–800 (2020).
21. Scaife, A. A. *et al.* Skillful long-range prediction of European and North American winters. *Geophys. Res. Lett.* **41**, 2514–2519 (2014).
22. Weisheimer, A. *et al.* The Signal-to-Noise Paradox in Climate Forecasts: Revisiting Our Understanding and Identifying Future Priorities. *Bull. Am. Meteorol. Soc.* **105**, E651–E659 (2024).
23. Chelton, D. B. & Xie, S.-P. Coupled Ocean-Atmosphere Interaction at Oceanic Mesoscales | Oceanography.
24. Minobe, S., Kuwano-Yoshida, A., Komori, N., Xie, S.-P. & Small, R. J. Influence of the Gulf Stream on the troposphere. *Nature* **452**, 206–209 (2008).
25. Ogawa, F., Nakamura, H., Nishii, K., Miyasaka, T. & Kuwano-Yoshida, A. Dependence of the climatological axial latitudes of the tropospheric westerlies and storm tracks on the latitude of an extratropical oceanic front. *Geophys. Res. Lett.* **39**, 2011GL049922 (2012).
26. Nakamura, H. *et al.* “Hot Spots” in the climate system—new developments in the extratropical ocean–atmosphere interaction research: a short review and an introduction. *J. Oceanogr.* **71**, 463–467 (2015).
27. Ma, X. *et al.* Importance of Resolving Kuroshio Front and Eddy Influence in Simulating the North Pacific Storm Track. *J. Clim.* **30**, 1861–1880 (2017).
28. Rodwell, M. J., Rowell, D. P. & Folland, C. K. Oceanic forcing of the wintertime North Atlantic Oscillation and European climate. *Nature* **398**, 320–323 (1999).
29. Watanabe, M. & Kimoto, M. Tropical-extratropical connection in the Atlantic atmosphere-ocean variability. *Geophys. Res. Lett.* **26**, 2247–2250 (1999).
30. Omrani, N.-E., Keenlyside, N. S., Bader, J. & Manzini, E. Stratosphere key for wintertime atmospheric response to warm Atlantic decadal conditions. *Clim. Dyn.* **42**, 649–663 (2014).
31. Omrani, N.-E. *et al.* Key Role of the Ocean Western Boundary currents in shaping the Northern Hemisphere climate. *Sci. Rep.* **9**, 3014 (2019).
32. Gallego, B. & Cessi, P. Decadal Variability of Two Oceans and an Atmosphere. *J. Clim.* **14**, 2815–2832 (2001).
33. Kelly, K. A. & Dong, S. The Relationship of Western Boundary Current Heat

- Transport and Storage to Midlatitude Ocean-Atmosphere Interaction. in *Geophysical Monograph Series* (eds. Wang, C., Xie, S. P. & Carton, J. A.) 347–363 (American Geophysical Union, Washington, D. C., 2013). doi:10.1029/147GM19.
34. Zhang, R. & Delworth, T. L. Impact of the Atlantic Multidecadal Oscillation on North Pacific climate variability. *Geophys. Res. Lett.* **34**, (2007).
  35. Kohyama, T. *et al.* The Gulf Stream and Kuroshio Current are synchronized. *Science* **374**, 341–346 (2021).
  36. Qiu, B., Chen, S., Schneider, N. & Taguchi, B. A Coupled Decadal Prediction of the Dynamic State of the Kuroshio Extension System. *J. Clim.* **27**, 1751–1764 (2014).
  37. Tatebe, H. *et al.* Description and basic evaluation of simulated mean state, internal variability, and climate sensitivity in MIROC6. *Geosci. Model Dev.* **12**, 2727–2765 (2019).
  38. Eyring, V. *et al.* Overview of the Coupled Model Intercomparison Project Phase 6 (CMIP6) experimental design and organization. *Geosci. Model Dev.* **9**, 1937–1958 (2016).
  39. Qiu, B. & Chen, S. Variability of the Kuroshio Extension Jet, Recirculation Gyre, and Mesoscale Eddies on Decadal Time Scales. *J. Phys. Oceanogr.* **35**, 2090–2103 (2005).
  40. Tamura, Y. & Tozuka, T. Dominant Forcing Regions of Decadal Variations in the Kuroshio Extension Revealed by a Linear Rossby Wave Model. *Geophys. Res. Lett.* **50**, e2023GL102995 (2023).
  41. Taguchi, B. *et al.* Decadal Variability of the Kuroshio Extension: Observations and an Eddy-Resolving Model Hindcast\*. *J. Clim.* **20**, 2357–2377 (2007).
  42. Sasaki, Y. N., Minobe, S. & Schneider, N. Decadal Response of the Kuroshio Extension Jet to Rossby Waves: Observation and Thin-Jet Theory\*. *J. Phys. Oceanogr.* **43**, 442–456 (2013).
  43. Kim, W. M., Yeager, S. G., Danabasoglu, G. & Chang, P. Exceptional multi-year prediction skill of the Kuroshio Extension in the CESM high-resolution decadal prediction system. *Npj Clim. Atmospheric Sci.* **6**, 118 (2023).
  44. Ham, Y.-G., Kug, J.-S., Park, J.-Y. & Jin, F.-F. Sea surface temperature in the north tropical Atlantic as a trigger for El Niño/Southern Oscillation events. *Nat. Geosci.* **6**, 112–116 (2013).

45. McGregor, S. *et al.* Recent Walker circulation strengthening and Pacific cooling amplified by Atlantic warming. *Nat. Clim. Change* **4**, 888–892 (2014).
46. Ruprich-Robert, Y. *et al.* Assessing the Climate Impacts of the Observed Atlantic Multidecadal Variability Using the GFDL CM2.1 and NCAR CESM1 Global Coupled Models. *J. Clim.* **30**, 2785–2810 (2017).
47. Sun, C. *et al.* Western tropical Pacific multidecadal variability forced by the Atlantic multidecadal oscillation. *Nat. Commun.* **8**, 15998 (2017).
48. Wu, C.-R., Lin, Y.-F. & Qiu, B. Impact of the Atlantic Multidecadal Oscillation on the Pacific North Equatorial Current bifurcation. *Sci. Rep.* **9**, 2162 (2019).
49. Baldwin, M. P. & Dunkerton, T. J. Stratospheric Harbingers of Anomalous Weather Regimes.
50. Baldwin, M. P. & Thompson, D. W. J. A critical comparison of stratosphere–troposphere coupling indices. *Q. J. R. Meteorol. Soc.* **135**, 1661–1672 (2009).
51. Kidston, J. *et al.* Stratospheric influence on tropospheric jet streams, storm tracks and surface weather. *Nat. Geosci.* **8**, 433–440 (2015).
52. Barsugli, J. J. & Battisti, D. S. The Basic Effects of Atmosphere–Ocean Thermal Coupling on Midlatitude Variability. (1998).
53. Mori, M. *et al.* Northern Hemisphere winter atmospheric teleconnections are intensified by extratropical ocean–atmosphere coupling. *Commun. Earth Environ.* **5**, 124 (2024).
54. Mori, M. *et al.* The Influence of Extratropical Ocean on the PNA Teleconnection: Role of Atmosphere–Ocean Coupling. *Geophys. Res. Lett.* **51**, e2024GL110234 (2024).
55. Taguchi, B. *et al.* Seasonal Evolutions of Atmospheric Response to Decadal SST Anomalies in the North Pacific Subarctic Frontal Zone: Observations and a Coupled Model Simulation. *J. Clim.* **25**, 111–139 (2012).
56. Okajima, S. *et al.* Mechanisms for the Maintenance of the Wintertime Basin-Scale Atmospheric Response to Decadal SST Variability in the North Pacific Subarctic Frontal Zone. *J. Clim.* **31**, 297–315 (2018).
57. Nishii, K., Nakamura, H. & Orsolini, Y. J. Geographical Dependence Observed in Blocking High Influence on the Stratospheric Variability through Enhancement and Suppression of Upward Planetary-Wave Propagation. *J. Clim.* **24**, 6408–6423 (2011).
58. Haarsma, R. J. *et al.* High Resolution Model Intercomparison Project

- (HighResMIP v1.0) for CMIP6. *Geosci. Model Dev.* **9**, 4185–4208 (2016).
59. Roberts, M. J. *et al.* The Benefits of Global High Resolution for Climate Simulation: Process Understanding and the Enabling of Stakeholder Decisions at the Regional Scale. *Bull. Am. Meteorol. Soc.* **99**, 2341–2359 (2018).
  60. Patrizio, C. R. *et al.* Improved Extratropical North Atlantic Atmosphere–Ocean Variability with Increasing Ocean Model Resolution. *J. Clim.* **36**, 8403–8424 (2023).
  61. Qiu, B., Chen, S. & Oka, E. Why Did the 2017 Kuroshio Large Meander Event Become the Longest in the Past 70 Years? *Geophys. Res. Lett.* **50**, e2023GL103548 (2023).
  62. Sato, H. *et al.* Impact of an unprecedented marine heatwave on extremely hot summer over Northern Japan in 2023. *Sci. Rep.* **14**, 16100 (2024).
  63. Hirahara, S., Ishii, M. & Fukuda, Y. Centennial-Scale Sea Surface Temperature Analysis and Its Uncertainty. (2014) doi:10.1175/JCLI-D-12-00837.1.
  64. Rayner, N. A. *et al.* Global analyses of sea surface temperature, sea ice, and night marine air temperature since the late nineteenth century. *J. Geophys. Res. Atmospheres* **108**, 2002JD002670 (2003).
  65. Pujol, M.-I. *et al.* DUACS DT2014: the new multi-mission altimeter data set reprocessed over 20 years. *Ocean Sci.* **12**, 1067–1090 (2016).
  66. Hersbach, H. *et al.* The ERA5 global reanalysis. *Q. J. R. Meteorol. Soc.* **146**, 1999–2049 (2020).
  67. Bretherton, C. S., Widmann, M., Dymnikov, V. P., Wallace, J. M. & Bladé, I. The Effective Number of Spatial Degrees of Freedom of a Time-Varying Field. (1999).
  68. Torrence, C. & Compo, G. P. A Practical Guide to Wavelet Analysis. (1998).
  69. Noh, Y. & Jin Kim, H. Simulations of temperature and turbulence structure of the oceanic boundary layer with the improved near-surface process. *J. Geophys. Res. Oceans* **104**, 15621–15634 (1999).
  70. Gent, P. R. & McWilliams, J. C. Isopycnal Mixing in Ocean Circulation Models. (1990).
  71. Yamagami, Y., Tatebe, H., Kataoka, T., Suzuki, T. & Watanabe, M. Impacts of Oceanic Mesoscale Structures on Sea Surface Temperature in the Arabian Sea and Indian Summer Monsoon Revealed by Climate Model Simulations. (2023) doi:10.1175/JCLI-D-22-0510.1.

72. Tatebe, H. & Watanabe, M. MIROC MIROC6 model output prepared for CMIP6 CMIP piControl. Earth System Grid Federation <https://doi.org/10.22033/ESGF/CMIP6.5711> (2018).
73. Yamagami, Y., Watanabe, M., Mori, M. & Ono, J. Barents-Kara sea-ice decline attributed to surface warming in the Gulf Stream. *Nat. Commun.* **13**, 3767 (2022).
74. Voldoire, A. CNRM-CERFACS CNRM-CM6-1 model output prepared for CMIP6 HighResMIP control-1950. Earth System Grid Federation <https://doi.org/10.22033/ESGF/CMIP6.3946> (2019).
75. Voldoire, A. CNRM-CERFACS CNRM-CM6-1-HR model output prepared for CMIP6 HighResMIP control-1950. Earth System Grid Federation <https://doi.org/10.22033/ESGF/CMIP6.3947> (2019).
76. Consortium (EC-Earth), E.-E. EC-Earth-Consortium EC-Earth3P model output prepared for CMIP6 HighResMIP control-1950. Earth System Grid Federation <https://doi.org/10.22033/ESGF/CMIP6.4547> (2019).
77. Consortium (EC-Earth), E.-E. EC-Earth-Consortium EC-Earth3P-HR model output prepared for CMIP6 HighResMIP control-1950. Earth System Grid Federation <https://doi.org/10.22033/ESGF/CMIP6.4548> (2018).
78. Roberts, C. D., Senan, R., Molteni, F., Boussetta, S. & Keeley, S. ECMWF ECMWF-IFS-LR model output prepared for CMIP6 HighResMIP control-1950. Earth System Grid Federation <https://doi.org/10.22033/ESGF/CMIP6.4946> (2018).
79. Roberts, C. D., Senan, R., Molteni, F., Boussetta, S. & Keeley, S. ECMWF ECMWF-IFS-MR model output prepared for CMIP6 HighResMIP control-1950. Earth System Grid Federation <https://doi.org/10.22033/ESGF/CMIP6.4947> (2018).
80. Roberts, M. MOHC HadGEM3-GC31-LL model output prepared for CMIP6 HighResMIP control-1950. Earth System Grid Federation <https://doi.org/10.22033/ESGF/CMIP6.5885> (2017).
81. Roberts, M. MOHC HadGEM3-GC31-MM model output prepared for CMIP6 HighResMIP control-1950. Earth System Grid Federation <https://doi.org/10.22033/ESGF/CMIP6.5888> (2017).
82. Qiu, B. & Kelly, K. A. Upper-Ocean Heat Balance in the Kuroshio Extension Region. (1993).
83. Moisan, J. R. & Niiler, P. P. The Seasonal Heat Budget of the North Pacific: Net

Heat Flux and Heat Storage Rates (1950–1990). (1998).

## **Methods**

### **Observational and Reanalysis data**

Monthly sea surface temperature (SST) data from the Centennial In Situ Observation-Based Estimates of the Variability of SST and Marine Meteorological Variables version 2 (COBE-SST2)<sup>63</sup> and the Hadley Centre Sea Ice and Sea Surface Temperature (HadISST)<sup>64</sup> were used for the period 1900–2023. Daily sea level anomaly (SLA) products from CMEMS (DUACS DT2014)<sup>65</sup> with a horizontal resolution of  $1/4^\circ \times 1/4^\circ$  were utilized for the period 1993–2023. ERA5<sup>66</sup> was used for geopotential height for the period 1979–2023.

### **Definitions of climate indices**

Gulf Stream and Kuroshio SST anomalies are defined as area-averaged SST anomalies over the North Atlantic ( $50^\circ\text{--}80^\circ\text{W}$ ,  $35^\circ\text{N--}45^\circ\text{N}$ ) and North Pacific ( $140^\circ\text{E--}170^\circ\text{E}$ ,  $35^\circ\text{N--}45^\circ\text{N}$ )<sup>35</sup>. NAM index is defined as the first EOF mode of zonal-mean daily geopotential height at each level<sup>49,50</sup> to examine the stratosphere-troposphere coupling. NAO index is also defined as the principal component for the first EOF mode of the geopotential height anomalies at 500hPa over the North Atlantic ( $60^\circ\text{W--}0^\circ$ ,  $30^\circ\text{N--}70^\circ\text{N}$ ). The subpolar gyre SST timeseries are calculated from area-averaged SST anomalies over  $40^\circ\text{W--}0^\circ$ ,  $55^\circ\text{N--}70^\circ\text{N}$ .

### **Statistical analysis**

For linear correlations and regressions, two-tailed t-test is adapted at 90% confidence level. Degree of freedom is estimated following Bretherton et al.<sup>67</sup> Singular value decomposition (SVD) is applied to SST anomalies in the North Pacific ( $120^\circ\text{E--}180^\circ\text{E}$ ,  $25^\circ\text{N--}55^\circ\text{N}$ ) and North Atlantic ( $30^\circ\text{W--}90^\circ\text{W}$ ,  $25^\circ\text{N--}55^\circ\text{N}$ ). Wavelet analysis<sup>68</sup> is applied to the SST timeseries.

### **Climate model simulations**

We used the sixth version of the Model for Interdisciplinary Research on Climate (MIROC6)<sup>37</sup>. The atmospheric component has a T85 spectral truncation, corresponding to a horizontal resolution of approximately 1.4° for both latitude and longitude. There are 81 vertical levels, with the model top at 0.004 hPa. The ocean component employs a tripolar coordinate system, with a longitudinal grid spacing of 1° and meridional grid spacing varying from 0.5° near the equator to 1° in the mid-latitudes, and 62 hybrid  $\sigma$ -z levels in the vertical direction. The surface mixed layer parameterization<sup>69</sup> and the parameterization for eddy isopycnal diffusion<sup>70</sup> are used in the ocean component. A high-resolution version of MIROC6, i.e., MIROC6subhires<sup>35,71</sup>, was also used. The atmospheric component remains the same, but the ocean horizontal resolution is increased to 0.25° × 0.25°, retaining the same vertical levels. The surface mixed layer parameterization is the same as in MIROC6, while the eddy isopycnal diffusion is not adapted from the equator to 60°N/ 60°S. After the model climate reached a quasi-equilibrium state in spin-up, an additional 200 (1000) yr-long integration was performed for MIROC6subhires (MIROC6<sup>72</sup>) with a preindustrial external forcing dataset as in CMIP6 protocol<sup>38</sup>. Hereafter, we refer the last 100-year output for MIROC6subhires (MIROC6) to CTL (CTL-LR) (Supplementary Table 1).

### **North Atlantic-Global Atmosphere and North Pacific-Global Atmosphere experiments**

To highlight the relative role of SST in the Kuroshio and Gulf Stream, we also conduct ensemble experiments using MIROC6subhires, in which modeled SST are restored to monthly SST from CTL with 15-day restoring timescale. The SST restoring is adapted over the North Atlantic (30°–75° W, 30°–50° N) for North Atlantic-Global Atmosphere (NAGA)<sup>73</sup> and North Pacific (130°–180° E, 30°–50° N) for North Pacific-Global Atmosphere (NPGA), respectively (Supplementary Table 1). The nudging flux is added to the surface heat flux to the ocean:

$$Nudging\ flux = \frac{\rho C_p h}{\tau} \times (SST_{CTL} - SST_{model}). \quad (1)$$

$\rho$  (=1027 kg m<sup>-3</sup>) is the density of the seawater,  $C_p$ (=4187 J kg<sup>-1</sup> K<sup>-1</sup>) is the specific heat of the seawater,  $\tau$  (= 15days) is the restoring time scale, and  $h$  (=50 m) is assumed to be surface mixed layer affected by SST restoring. The restored SST anomaly linearly



decreases to 0 within 6 degrees outside nudging areas (Supplementary Fig. 2). Initial conditions are taken from CTL with more than 10-year interval. Both integrations are performed for 100-year and 5 ensemble members under the preindustrial condition as in CTL.

SST-restoring for North Atlantic and North Pacific are also conducted for MIROC6, which are referred to as NAGA-LR and NPGA-LR, respectively. The comparison between the ensemble mean of each experiment and CTL enables us to evaluate how the forcings of Kuroshio and Gulf Stream SST account for global climate variability. We note that SSTs in CTL are converted to the atmospheric horizontal resolution before the nudging flux are calculated. Therefore, the SST-restoring is expected to constrain the basin-scale SST variability rather than oceanic mesoscale variability.

### **No Indo-Pacific SST variability experiment**

To assess the impact of tropical SST forcing (e.g., ENSO and IOD), additional simulations suppressing SST anomalies in the tropical Indian and Pacific Oceans (NoINPAC) were conducted. Two sets of experiments are performed with SST-restoring to the climatology in CTL over the entire tropical Indian Ocean and Pacific Ocean (Supplementary Fig. 2). One is the preindustrial control-type simulation without the SST-restoring in the North Atlantic (CTL-NoINPAC). The other is the ensemble simulation with constraining SST anomalies in the North Atlantic (NAGA-NoINPAC) (Supplementary Table 1).

### **Sensitivity experiments by the atmospheric model**

Atmospheric responses to SST anomalies in the Gulf Stream region were investigated using the atmospheric component of MIROC6 and MIROC6subhires (Supplementary Table 2). In the control run (AGCM-Clim), the atmospheric model is forced by the monthly climatology of SST and sea ice concentration for CTL. SST anomalies are added over the global ocean (AGCM-Global\_SST) and North Atlantic (30°–75° W, 30°–50° N; AGCM-Gulf\_SST). The SST anomalies are defined as the linear regression to the area-averaged SST timeseries in the Gulf Stream region (50°–80°W, 35°N–45°N) in CTL (Supplementary Fig. 10). The unit of SST anomalies are comparable to those when the Gulf Stream SST is +1°C. The difference between AGCM-Global\_SST (AGCM-

Gulf\_SST) and AGCM-Clim indicates the impact of the SST anomalies over the global ocean (Gulf Stream region). All experiments are integrated for 5 years with 10-member ensembles with the initial condition taken from CTL with more than 10-year interval and the last 4-year outputs are analyzed.

### **CMIP6 simulations**

CMIP6 multi-model ensemble data were analyzed to explore the relationship between North Atlantic SST and Northern Hemisphere atmospheric circulation. Control-1950 experiments from HighResMIP<sup>58</sup> are investigated so that the external forcing is excluded. Models which have the non-eddy and eddy-permitting ocean component are selected, i.e., CNRM-CM6-1<sup>74</sup>, CNRM-CM6-1-HR<sup>75</sup>, EC-Earth3P<sup>76</sup>, EC-Earth3P-HR<sup>77</sup>, ECMWF-IFS-LR<sup>78</sup>, ECMWF-IFS-MR<sup>79</sup>, HadGEM3-GC31-LL<sup>80</sup>, and HadGEM3-GC31-MM<sup>81</sup> (Supplementary Table. 3).

### **Ocean mixed layer heat budget**

The temperature balance within the ocean mixed layer are examined<sup>73,82,83</sup>:

$$\frac{\partial T_m}{\partial t} = \frac{Q_{net} - q_d}{\rho C_p H} - OCN \quad (3).$$

$T_m$  means temperature averaged over the mixed layer. The first term on the right-hand side is the contribution from the surface heat flux, where  $Q_{net}$  is the net surface heat flux,  $q_d$  is the downward solar insolation penetrating through the bottom of the mixed layer,  $\rho$  ( $=1027 \text{ kg m}^{-3}$ ) is the density of the seawater,  $C_p$  ( $=4187 \text{ J kg}^{-1} \text{ K}^{-1}$ ) is the specific heat of the seawater, and  $H$  is the mixed layer depth. We define  $H$  as a depth where the density is  $0.125 \text{ kg m}^{-3}$  higher than the surface density. The second term is oceanic contribution including the horizontal advection and entrainment through the bottom boundary of the mixed layer, which is estimated from the residual between the temperature tendency and atmospheric contribution.

### **Data availability**

The HadISST dataset was downloaded from the Met Office website (<https://www.metoffice.gov.uk/hadobs/hadisst/>). The COBE-SST2 dataset was downloaded from the NOAA Physical Sciences Laboratory website

(<https://psl.noaa.gov/data/gridded/data.cobe2.html>). The altimeter products were produced and distributed by Copernicus Marine Environment Monitoring Service (<http://marine.copernicus.eu>). ERA5 data was downloaded from ECMWF (<https://doi.org/10.24381/cds.f17050d7>). The CMIP6 historical experimental dataset was downloaded from the ESGF website (<https://esgf-node.llnl.gov/projects/cmip6/>). The Model outputs generated in this study are available from the corresponding author upon reasonable request.

### **Code availability**

The model code is available under restricted access for the developers' policy, access can be obtained by contact with the corresponding author upon reasonable request.

### **Acknowledgements**

We thank the helpful comments by Hisashi Nakamura, Fumiaki Ogawa, and Masahiro Watanabe. This work is supported by MEXT program for the advanced studies of climate change projection (SENTAN) Grant Number JPMXD0722680395 (Y.Y., H.T., T.K., S.K., S.O.), and JSPS KAKENHI Grant Number JP20H05729 (Y.Y.), JP22H04487 (Y.Y., T.K., S.K.), JP22K14098 (Y.Y.), and JP24H00280 (Y.Y., H.T., S.K.). The model simulations were performed using Earth Simulator at the Japan Agency for Marine-Earth Science and Technology (JAMSTEC), Japan.

### **Author contributions**

Y.Y. conceived this study, conducted simulations, performed the analysis, and wrote the first draft. H.T. lead the MIROC6 and MIROC6subhires models development. Y.Y., H.T., T.K., S.K., and S.O. discussed the results and contributed to the manuscript.

### **Competing interests**

The authors declare no competing interests.

## Supplementary figures and Tables

Name	Ocean nominal resolution	SST-restoring			Ensemble member	Period [year]
		Gulf Stream	Kuroshio	Tropics		
CTL	0.25°	Free	Free	Free	1	100
NAGA	0.25°	CTL	Free	Free	5	100
NPGA	0.25°	Free	CTL	Free	5	100
CTL-LR	1.0°	Free	Free	Free	1	100
NAGA-LR	1.0°	CTL	Free	Free	5	100
NPGA-LR	1.0°	Free	CTL	Free	5	100
CTL- NoINPAC	0.25°	Free	Free	CTL Clim	1	100
NAGA- NoINPAC	0.25°	CTL	Free	CTL Clim	5	100

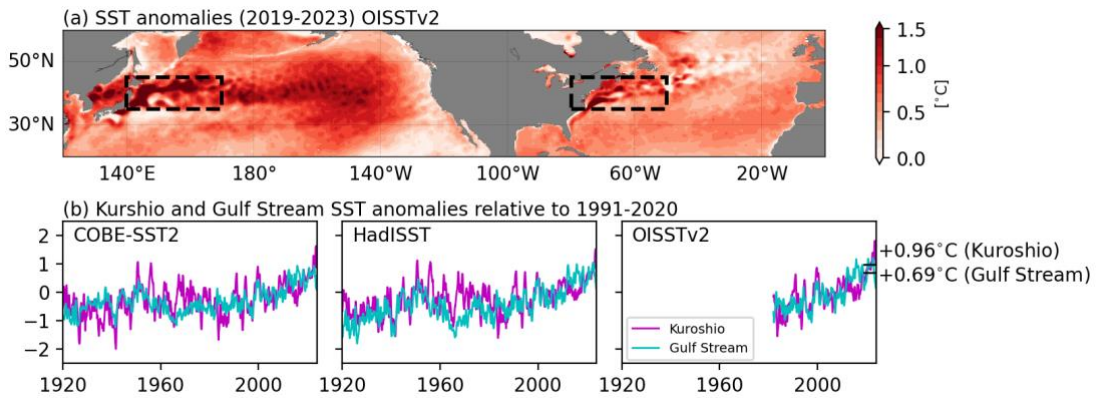
**Supplementary Table 1.** Summary of numerical experiments using coupled models. “Free” for Gulf Stream, Kuroshio, and Tropics indicate that SST evolve freely without any SST-restoring, while “CTL Clim” for Tropics means equatorial SST are nudged to climatological SST in CTL. The areas of SST-nudging for experiments are shown in Supplementary Figure 1 and 2.

Name	Prescribed SST anomalies			Ensemble member	Simulation years
	Gulf Stream	Kuroshio	Tropics		
AGCM- Clim	No	No	No	10	5
AGCM- Global_SST	Yes	Yes	Yes	10	5
AGCM- Gulf_SST	Yes	No	No	10	5

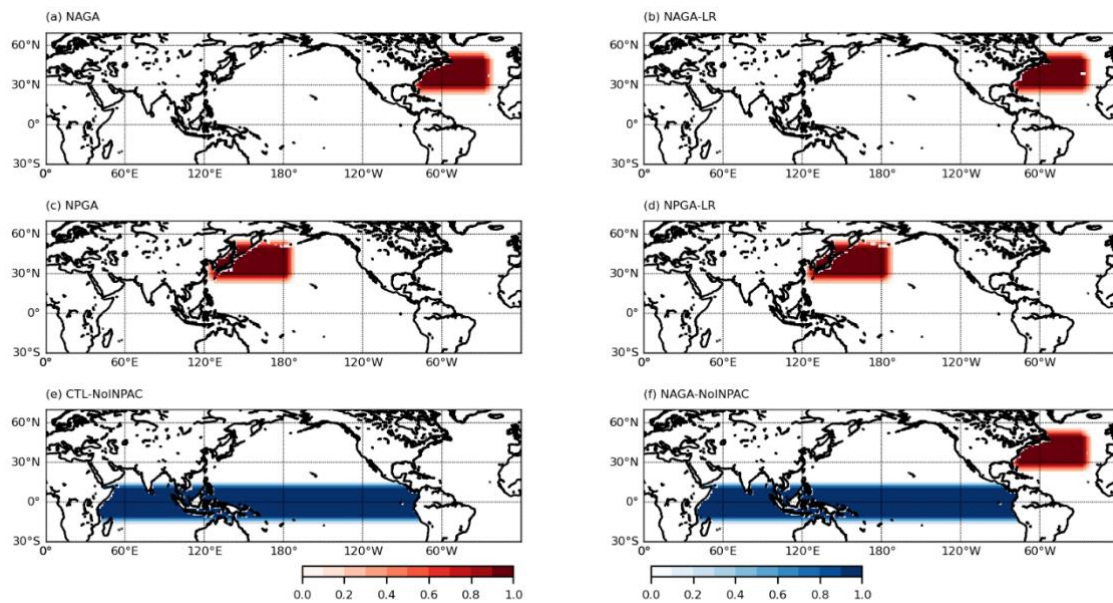
**Supplementary Table 2.** Summary of AGCM sensitivity experiments.

model	Ocean nominal resolution [km]	variant-id
CNRM-CM6-1	100	r1i1p1f2
CNRM-CM6-1-HR	25	r1i1p1f2
EC-Earth3P	100	r1p1i1f2
EC-Earth3P-HR	25	r1p1i1f2
ECMWF-IFS-LR	100	r1p1i1f1
ECMWF-IFS-MR	25	r1p1i1f1
HadGEM3-GC31-LL	100	r1p1i1f1
HadGEM3-GC31-MM	25	r1p1i1f1

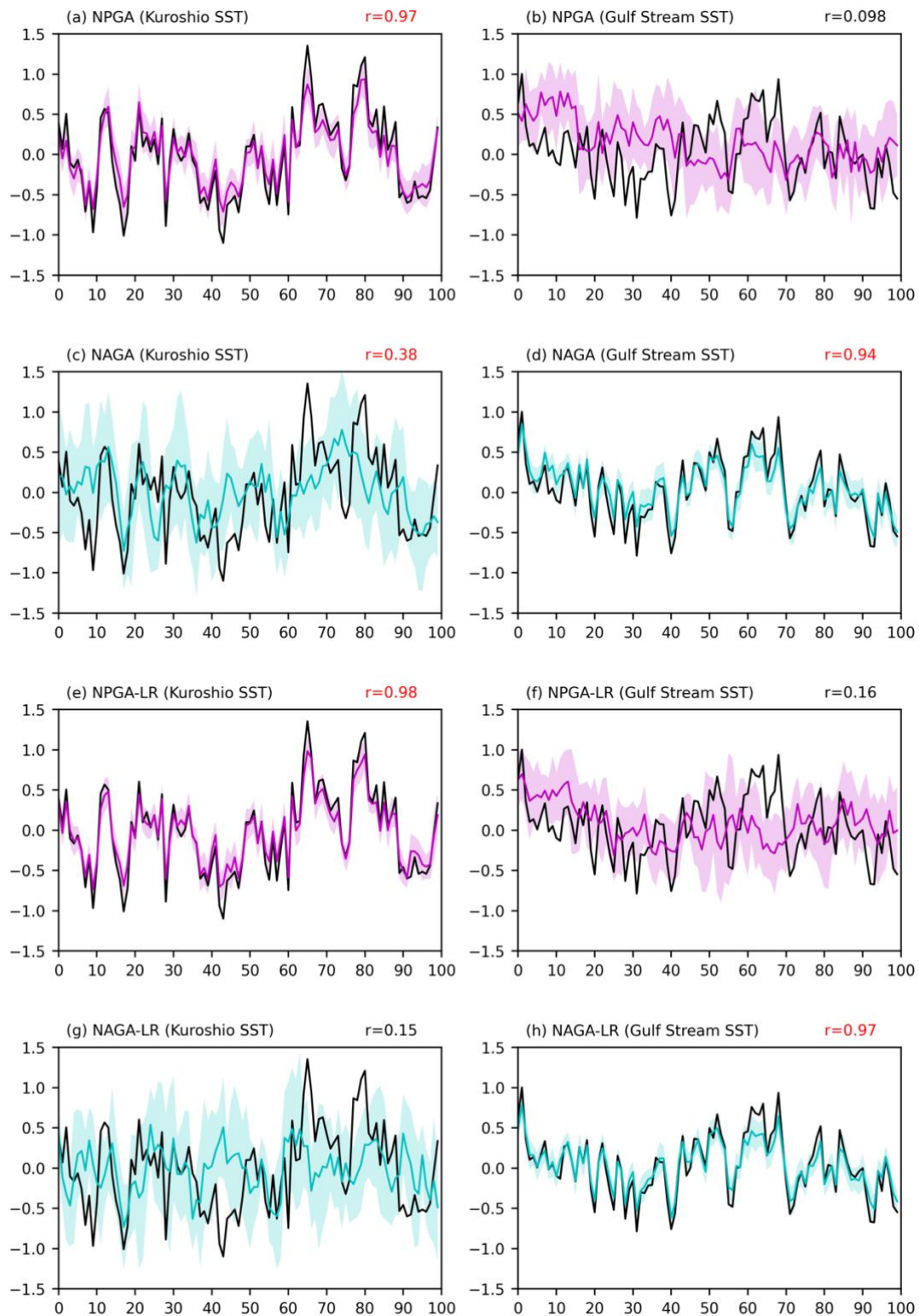
**Supplementary Table 3.** List of HighResMIP model name, nominal ocean horizontal resolution [km], and variant-id analyzed in this study.



**Supplementary Figure 1. Abnormally warm sea surface temperature (SST) over the Northern Hemisphere during recent years.** **a** Observed SST anomalies relative to the annual mean during 1991-2020. **b** Annual-mean SST anomalies relative to 1991-2020 area-averaged over the Kuroshio (140°E-170°E, 35°N-45°N; magenta) and Gulf Stream (50°-80°W, 35°N-45°N; cyan) regions for the different observational datasets. 2019-2023 values for OISSTv2 are shown in the right panel.



**Supplementary Figure 2. SST-restoring region for each experiments. a** Factors which are multiplied to the nudging heat flux in NAGA. 1 (0) means the The restored SST anomaly linearly decreases to 0 within 6 degrees outside nudging areas. **b-f** As in **a**, but for (b) NAGA-LR, (c) NPGA, (d) NPGA-LR. **e** As in **a**, but for the nudging heat flux for CTL-NoINPAC. Blue colors means that SST are restored to SST climatology in CTL. **f** As in **e**, but for NAGA-NoINPAC. Blue (red) colors indicate that the SST (SST anomalies) are restored to the SST climatology (anomalies) in CTL.

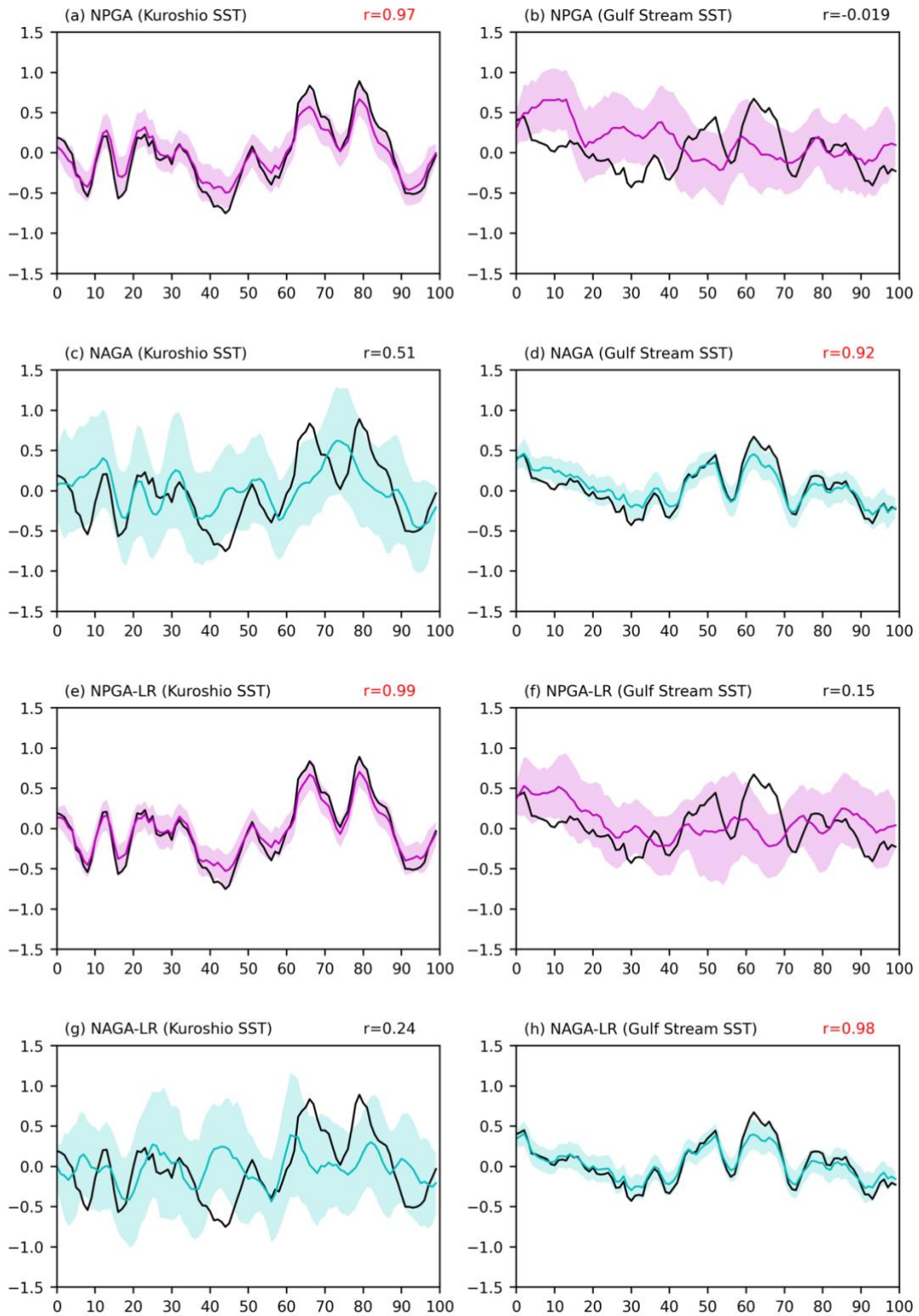


**Supplementary Figure 3 Simulated time series for Kuroshio and Gulf Stream SST.**

**a** Annual mean SST anomalies averaged over the Kuroshio region (140°E-170°E, 35°N-

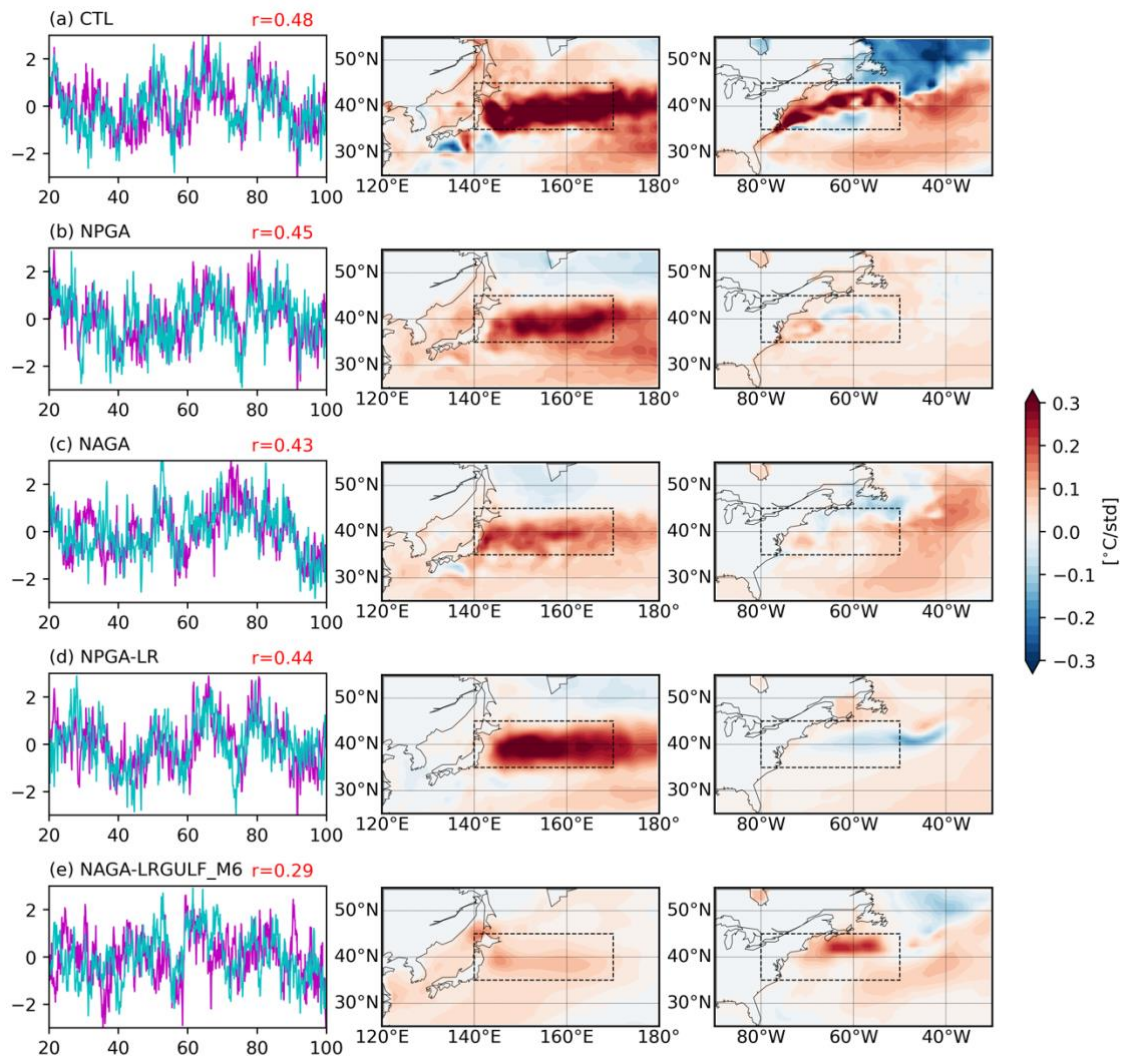
45°N; the region is indicated with a box in Fig.1 g-j) based on CTL (black) and the ensemble means for NPGA (magenta). Shading indicates one standard deviation of ensemble members in both experiments. Correlation coefficient for CTL and the ensemble mean of NPGA is shown in the upper right, with red colors indicating the statistically significant at 90% confidence level. **b** As in **a**, but for SST anomalies averaged over the Gulf Stream region (30°–80° W, 30°–50° N; black box in Fig.1 g-j). **c-h** As in **a,b**, but for (c),(d) NAGA, (e),(f) NPGA-LR, and (g),(h) NAGA-LR.



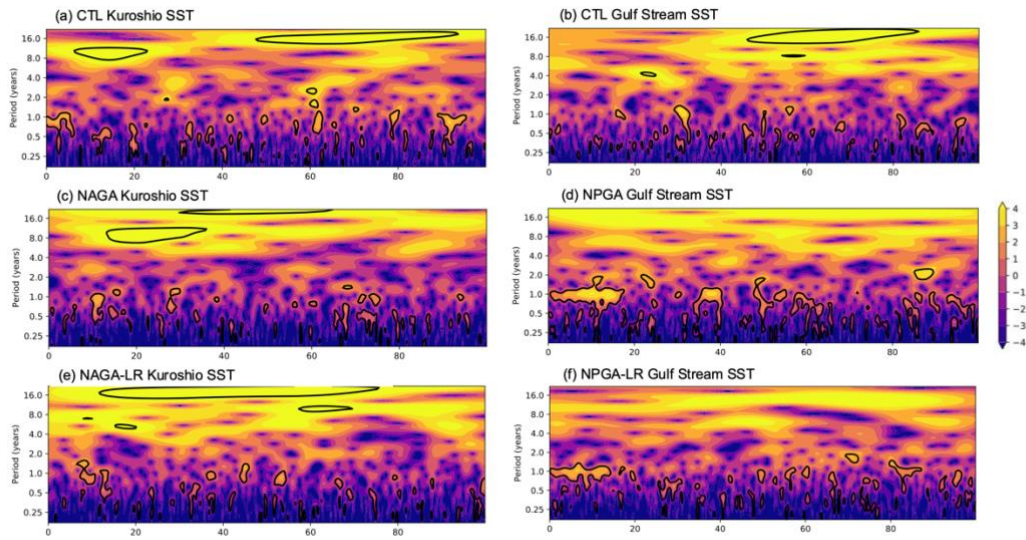


**Supplementary Figure 4 Simulated time series for the low-passed Kuroshio and Gulf Stream SST.** As in Supplementary Figure 3, but for 5-year running means.

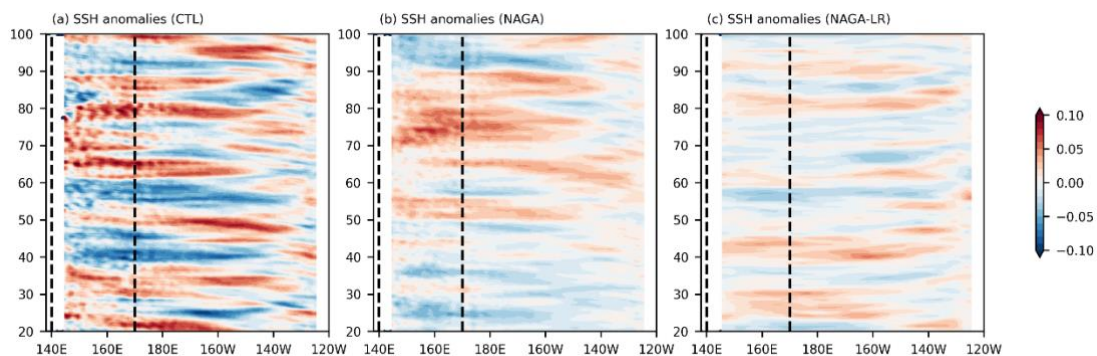




**Supplementary Figure 5. Dominant co-variability of Kuroshio and Gulf Stream SSTs.** (a) (left) Projected monthly SST time series on the first mode of the SVD (SVD1) between SST anomalies over the North Pacific (25°N-55°N, 120°E-180°) and North Atlantic (25°N-55°N, 90°W-30°W) for CTL. Correlation coefficient is also shown for the two time series and red colors indicates the statistically significant at 90%. (middle) SST patterns extracted as regressions on the normalized SVD1 in the North Pacific. (right) SST patterns extracted as regressions on the normalized SVD1 in the North Atlantic. **b-e** As in **a**, but for **b** NPGA, **c** NAGA, **d** NPGA-LR, and **e** NAGA-LR.



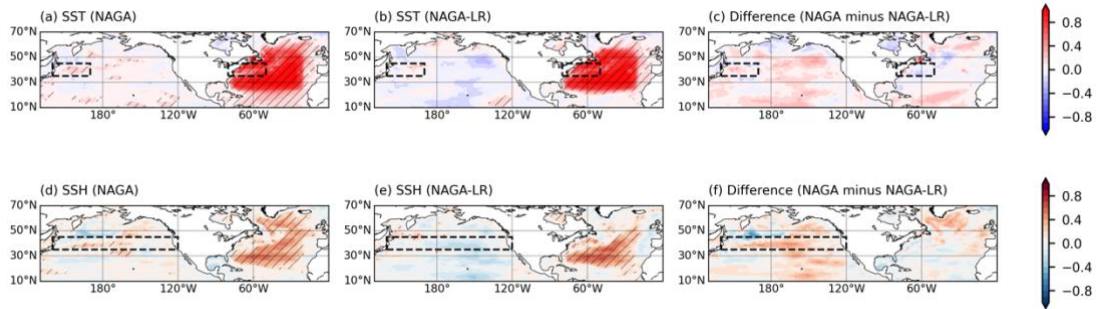
**Supplementary Figure 6. Normalized wavelet power spectrum for the SST anomalies in the Kuroshio and Gulf Stream.** **a,b** Normalized wavelet power spectrum (shade), significance level at 95% confidence level (contour), and cone of influence (hatching) for **(a)** Kuroshio and **(b)** Gulf Stream SST anomalies in CTL. The vertical axis is the period scale in logarithmic [year], while the horizontal axis is the simulation year. **c,d** As in **a,b**, but for the ensemble means of **(c)** Kuroshio SST anomalies for NAGA and **(d)** Gulf Stream SST anomalies for NPGA. **e,f** As in **c,d**, but **(e)** Kuroshio SST anomalies for NAGA-LR and **(f)** Gulf Stream SST anomalies for NPGA-LR.



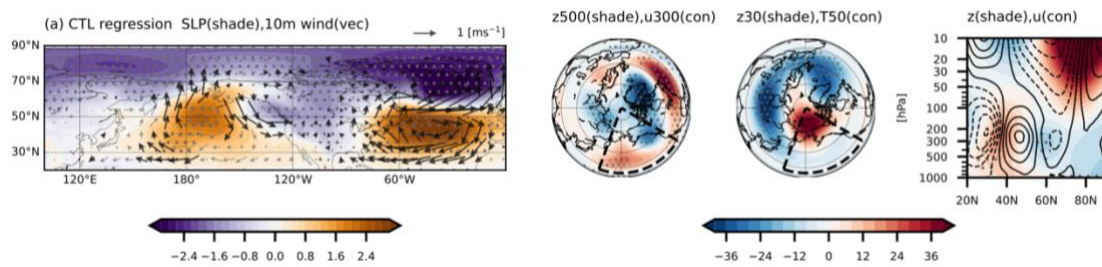
**Supplementary Figure 7. Comparison of westward propagation signals of SSH anomalies.** As in Fig. 2b, but for SSH anomalies [m] for **(a)** CTL, **(b)** NAGA, and **(c)** NAGA-LR averaged over 35°N-45°N. 13-month running mean are applied to the SSH



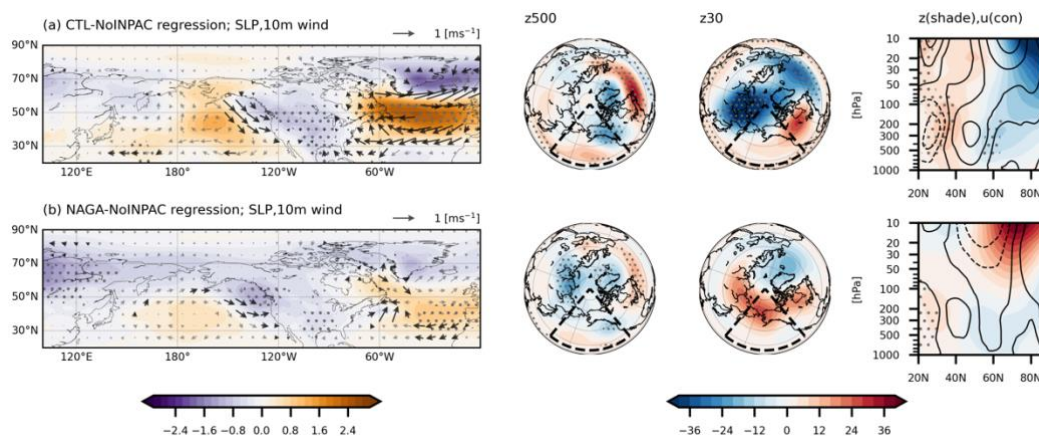
anomalies. Dashed lines indicate the Kuroshio region define in this study ( $140^{\circ}\text{E}$ - $170^{\circ}\text{E}$ ,  $35^{\circ}\text{N}$ - $45^{\circ}\text{N}$ ).



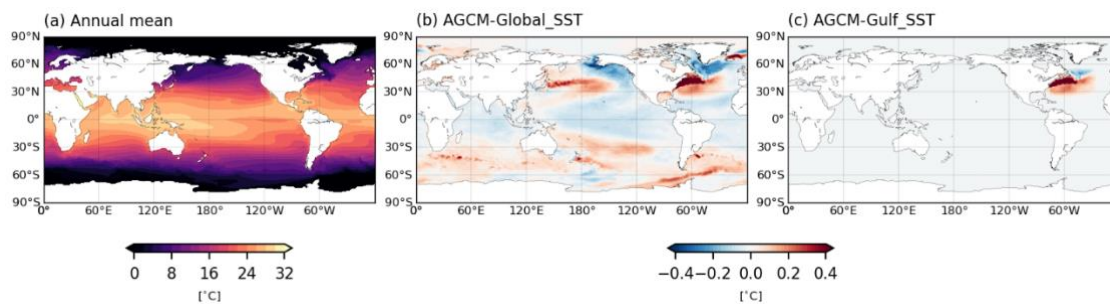
**Supplementary Figure 8. Reproduction of SST and SSH anomalies in NAGA and NAGA-LR. a** Point-to-point correlation coefficient of SST anomalies between CTL and the ensemble mean of NAGA. Hatching indicates statistically significant correlation at 90% confidence level. **b** As in **a**, but for NAGA-LR. **c** As in **a,b**, but for difference of correlation coefficients between NAGA and NAGA-LR. **d-f** As in **a-c**, but for SSH anomalies.



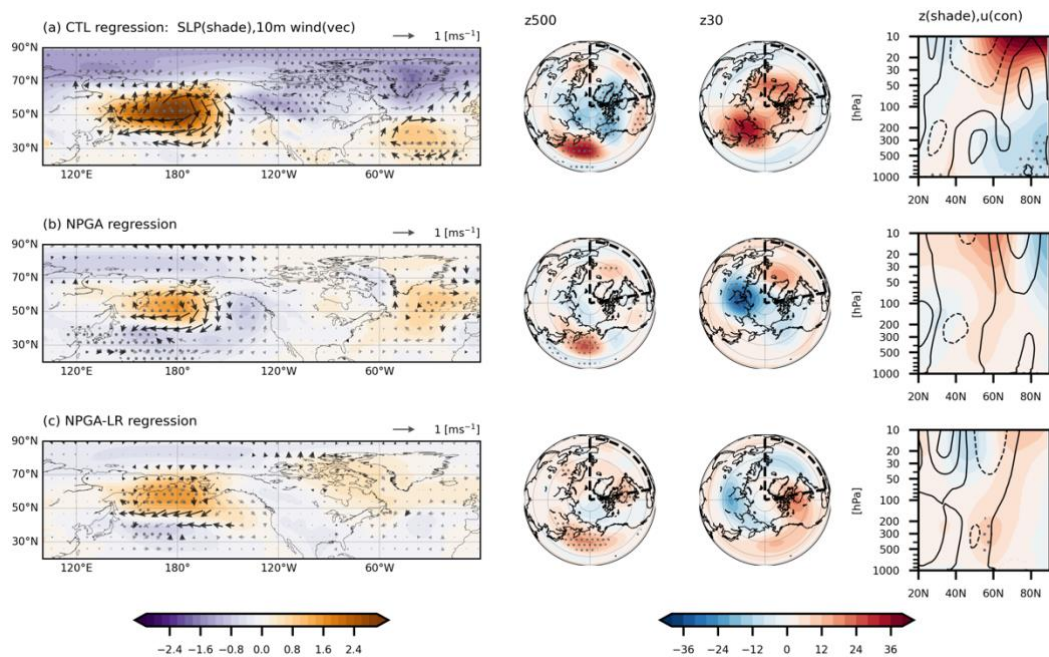
**Supplementary Figure 9. Response of the surface, tropospheric, and stratospheric circulation anomalies associated with the Gulf Stream SST anomalies for CTL. As in Fig. 3, but for CTL.**



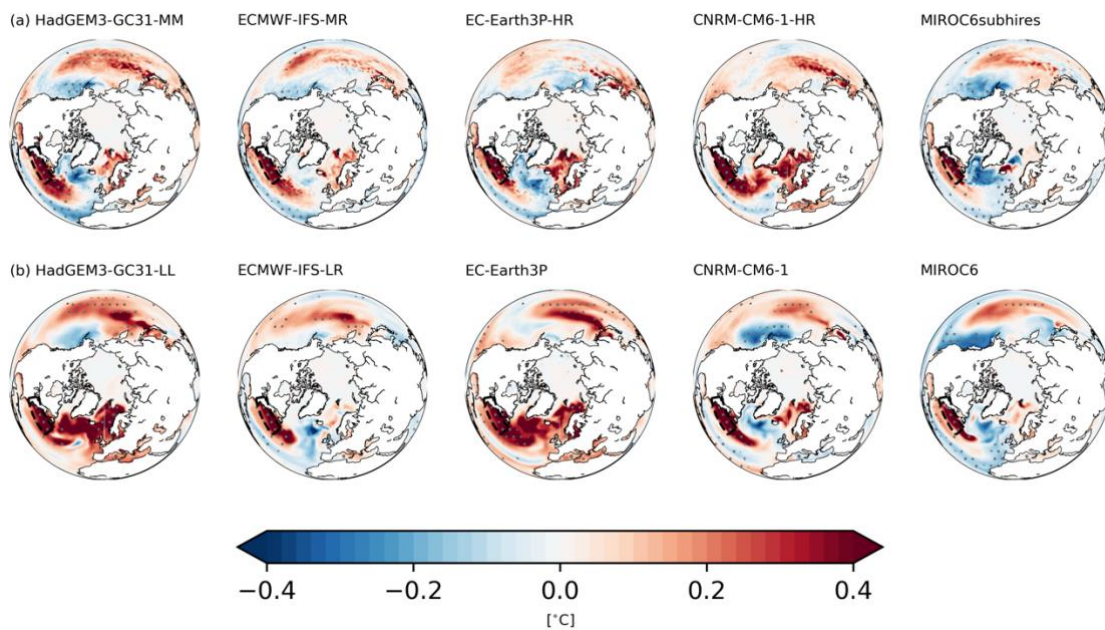
**Supplementary Figure 10. Response of the surface, tropospheric, and stratospheric circulation anomalies associated with the Gulf Stream SST anomalies for NoINPAC experiments. As in Fig. 3, but for (a) CTL-NoINPAC and (b) NAGA-NoINPAC.**



**Supplementary Figure 11. SST anomalies are prescribed to the AGCM experiments. a** Annual mean of SST prescribed to AGCM-Clim. Climatological SSTs are calculated from CTL. **b,c** SST anomalies prescribed to (b) AGCM-Global\_SST and (c) AGCM-Gulf\_SST. SST anomalies are defined by the regression coefficients of SST anomalies to the Gulf Stream SST for CTL. The unit is °C, indicating that the SST anomalies are comparable to those when the Gulf Stream SST is +1°C.



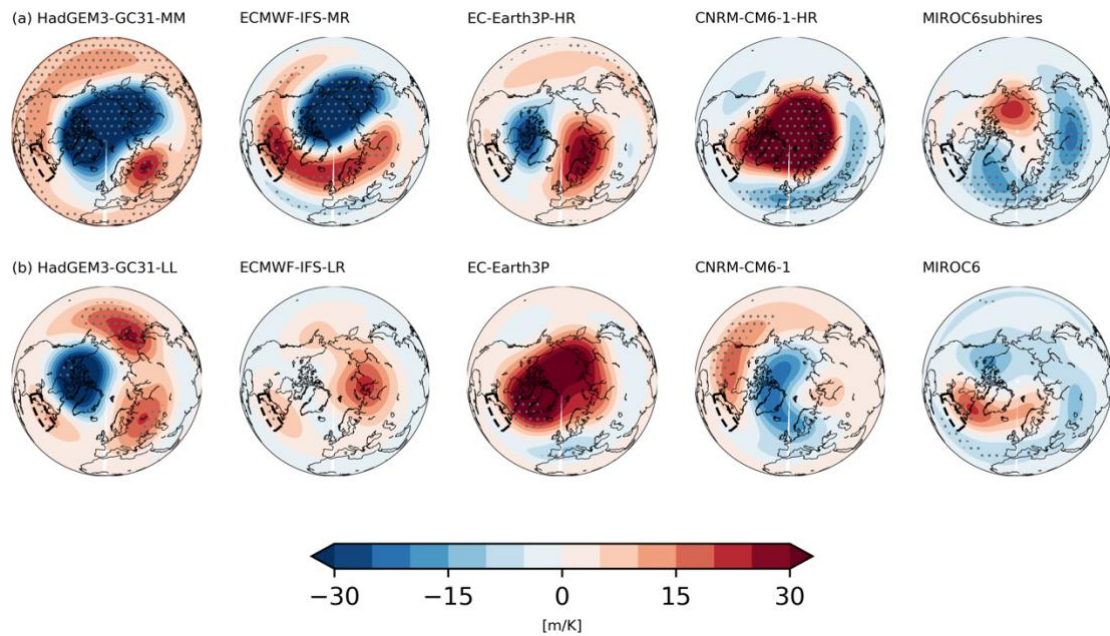
**Supplementary Figure 12. Response of the surface, tropospheric, and stratospheric circulation anomalies associated with the Kuroshio SST anomalies.** As in Fig.3 but for (a) CTL, (b) NPGA, and (c) NPGA-LR. All variables are regressed to the DJF mean SST anomalies in the Kuroshio.



**Supplementary Figure 13. Resolution dependence of the SST response to the Gulf Stream SST anomalies for CMIP6 models.** As in Figure 4, but for SST anomalies

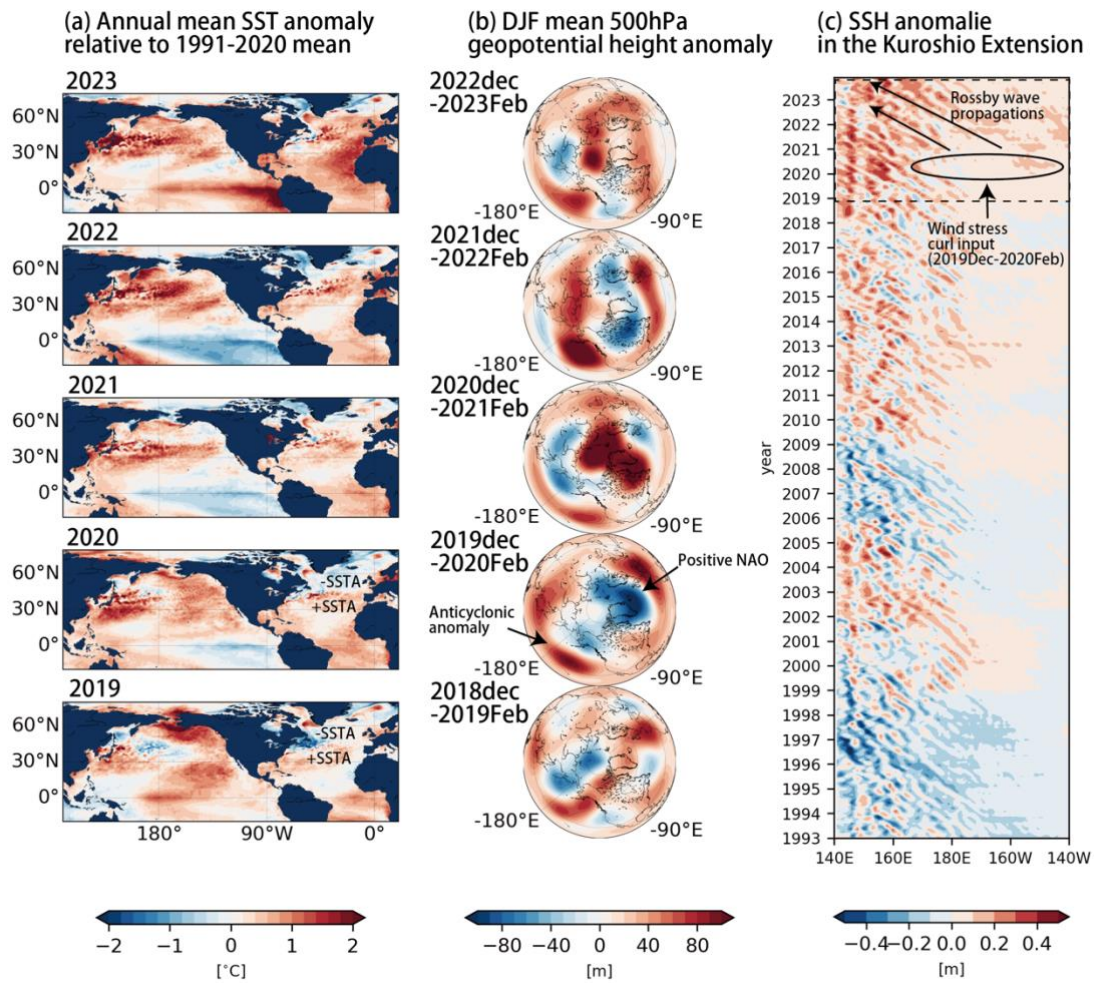


regressed to the Gulf Stream SST anomalies.



**Supplementary Figure 14. Resolution dependence of the upper tropospheric circulation response to the Gulf Stream SST anomalies for CMIP6 models.** DJF mean geopotential height at 30hPa [m/K] regressed to the DJF mean SST anomalies in the Gulf Stream (black dashed box) for CMIP6 models with (a) eddy-permitting and (b) non-eddy-permitting ocean model resolution. Dots indicate the statistically significant regression coefficients.





**Supplementary Figure 15. Observational evidence for the recent SST anomalies, atmospheric circulation anomalies in the Northern Hemisphere, and SSH anomalies in the Kuroshio Extension.** (a) Annual mean SST anomalies relative to 1991-2020 mean for OISSTv2 from 2019 to 2023. (b) DJF-mean geopotential height anomalies at 500hPa for ERA5. The anomalies are defined as the deviation from the climatology for 1991-2020. (c) Observed SSH anomalies in the Kuroshio Extension (32-36°N) for CMEMS. SSH anomalies calculated as the deviations from the climatology for 1993-2020.